Fluidic Control of a Turret Wake,

Part II: Aero-Optical Effects

Stanislav Gordeyev, Eric Jumper,
Department of Aerospace and Mechanical Engineering,
University of Notre Dame, Notre Dame, IN 46556

Bojan Vukasinovic, Ari Glezer,
Woodruff School of Mechanical Engineering,
Georgia Institute of Technology, Atlanta, GA 30332-0405

Valdis Kibens
The Boeing Company, MC S306-4030,
P.O. Box 516, Saint Louis, MO 63166

This paper, along with a companion paper [1], investigates the effects of flow control actuation on aero-optical distortions in the near wake of a 0.6 meter in diameter hemisphere-on-cylinder turret model placed on the side wall of a wind tunnel. The aero-optical environment was characterized using a Malley probe. The main objective of the current work was to assess the effectiveness of the active flow control in mitigating optical aberrations over a conformal optical window mounted on the turret for backward-looking elevation angles at subsonic Mach numbers. The paper presents the analysis of the aero-optical environment present for the baseline flow around the turret and the influence of that the different active-flow-control configurations have on that environment.

I.   Background

TURRETS provide convenient ways of pointing and tracking laser beams from airborne platforms; however, the turret creates a separated turbulent region of the flow, which, even at relatively-low subsonic speeds, starts to distort an otherwise planar emerging laser beam [2-4]. This, in turn, leads to the laser beam's unsteady defocus and jitter at the target [5]. The turbulent flow behind the turret is, in general, quite complex [4] and hard to control. However, it has been shown [2,4,6] that the main cause of aero-optical distortions for moderate back-looking angles is the shear-layer structures that form shortly after the flow separates from the hemispherical portion of the turret. One way to reduce the aero-optical degradation on the laser beam at these angles is to delay separation by manipulating the boundary layer just upstream of where separation would be in the absence of flow control. Recently, this approach was successfully demonstrated on a 0.25 meter hemispherical turret [7] where synthetic jet-actuators mounted flush on the hemispherical surface were able to delay the separation, reducing levels of optical distortion by as much as 45% for M=0.4.

Similar, but more powerful, synthetic-jet actuators were tested on a generic hemisphere-on-cylinder turret to see whether they could reduce optical aberrations behind a larger, 0.6 meter in diameter turret. The companion paper [1] discusses in detail the actuators' design, their locations on the turret and actuation cases tested, as well as actuation effects on surface pressure and wake velocity profiles for different actuation cases. This paper complements that paper and focuses on aero-optical measurements using a Malley probe.

II.   Experimental Setup and Procedures

Optical measurements around a 0.6 meter, hemisphere-on-cylinder turret using a Malley probe were performed in the Subsonic Aeronautical Research Laboratory (SARL) wind tunnel at Wright-Patterson AFB. The main objective of these tests was to obtain optical results for baseline (no actuation) and controlled (actuation) cases for several elevation angles and Mach numbers and to estimate the optical effectiveness of the flow control. The tunnel blockage imposed by the turret was 4.2%. To minimize tunnel-induced mechanical vibrations and relative motion between the turret and the optical bench, inner-tube isolators were placed between the optical table and trusses holding the optical bench, see Figure 1, left; these were effective in reducing the bench's vibrational motion.

Optical measurements were performed in the turret center-plane (i.e. zenith plane) at elevation angles from the oncoming flow of 129, 137, 143 and 148 degrees, see Figure 1, right; These angles were chosen because fluid-mechanic measurements had shown that, in the absence of forcing, the flow would be separated by 120 degrees. Measurements at each elevation angle were made at tunnel Mach numbers of 0.3, 0.4 and 0.5 using a Malley probe. The Malley probe is described in detail in [2]; it uses two parallel, small-aperture laser beams to measure one-dimensional slices of optical wavefronts in the streamwise direction. Regular Plexiglas windows in the tunnel walls ordinarily would be unacceptable for making optical measurements; however, the Malley probe was able to make excellent optical measurements through these windows because they did not impose significant optical distortions on the small, 1 mm, Malley-probe beams. A one-inch-diameter return mirror was mounted flush on the turret; the two Malley probe He-Ne laser beams were transmitted into the test section using a series of steering mirrors and, after reflecting off the turret-mounted return mirror, were reflected back to the optical bench along the same optical path. This approach to making Malley probe measurements allows the laser beams to go along the same measurement line twice, doubling the signal-to-noise ratio and significantly simplifying the optical set-up.
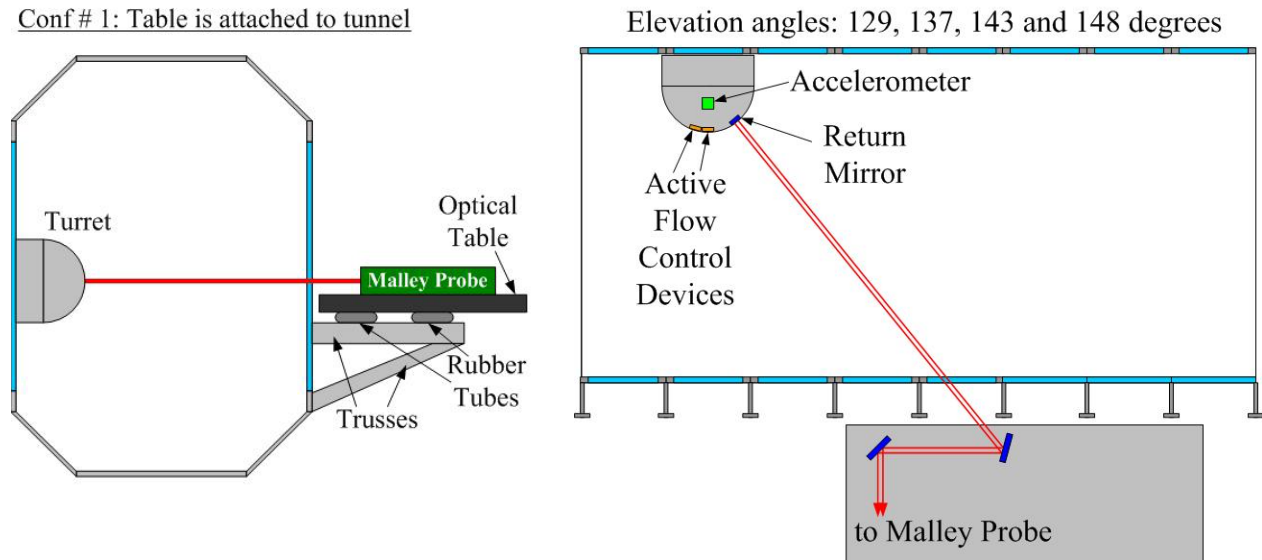

Figure 1. Optical table arrangement, side (left) and top (right) views.

The Malley-probe laser beams were separated by approximately 7 mm in the streamwise direction. Optical aberrations at selected elevation angles were measured by recording high-bandwidth, time-resolved deflection angles (jitter) of the laser beams using position sensing devices. The sampling frequency used was 50 kHz, and sampling times of 20 seconds were made for each measurement case.

The Malley probe data were processed as follows:

1. Measure streamwise deflection jitter angles $\theta_1(t)$ and $\theta_2(t)$.
2. Compute a cross-correlation function $S(f)$, $S(f) = \left\langle \hat{\theta}_1^*(f)\hat{\theta}_2(f) \right\rangle$, where square brackets denote ensemble averaging and asterisk denotes complex conjugate.

3. Calculate convective speed, U_c, by calculating the time delay between the two jitter signals using the spectral method described in Ref. [2].

4. Compute jitter power spectra $P_\theta(f) = \left\langle \left| \hat{\theta}(f) \right|^2 \right\rangle$ for each jitter signal.

5. Remove vibration contamination by analyzing the jitter-angle spectra $P_\theta(f)$ and applying a high-pass filter $F(f)$, as described below.

6. Calculate a time varying 1-D wavefront slice, OPD(t), assuming the frozen-flow hypothesis,

$$OPD(t) = -U_c \int \theta_1(t)dt$$

7. Apply an aperture, A_p, to $OPD(t)$ results, remove instantaneous tilt components from each apertured slice and calculate the residual OPD_{rms} average over all ensembles for a given aperture.

For results presented below, an aperture size, Ap, was chosen to be 1/3 of the hemisphere diameter, $Ap = 0.2$ m.
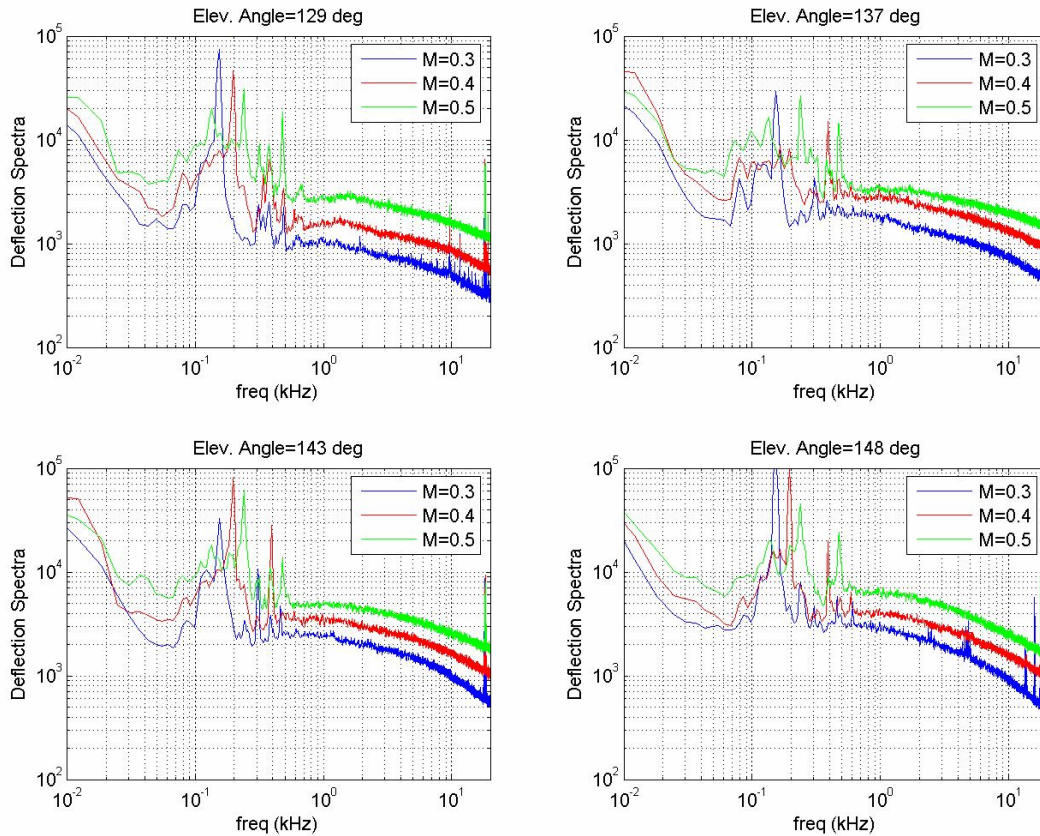

Figure 2. Optical deflection/jitter-angle spectra for different elevation angles as a function of the incoming Mach numbers. The horizontal axis is frequency in kHz.

III.   Results

A.   Baseline optical results.

   Baseline (i.e., turret with no active flow control) Malley probe jitter/beam-deflection-angle spectra for different elevation angles as a function of the incoming Mach number are presented in Figure 2. The series of peaks at low frequencies, below 500 Hz, is the result of mechanical vibrations of the tunnel, the turret, and to a lesser degree the optical bench. The main vibrational peak is related to the tunnel shaft rotation speed which was approximately 155 Hz for M = 0.3, 200 Hz for M = 0.4 and 250 Hz for M = 0.5. These vibrations completely overwhelm the optical signal at these frequencies and make the data unusable at these frequencies. Above 500 Hz the optical signal shows a broad hump which indicates the presence of the shear layer behind the turret. For the elevation angle of 129 degrees, the frequency location of this hump increases from approximately 1 kHz to 2 kHz, increasing with Mach

number. This characteristic is expected for the shear layer, confirming the fluid-mechanic conclusion that, in the absence of flow control, the Malley-probe beams encounter separated flow at the smallest of the four elevation angles. The corresponding Strouhal number was found to be approximately St = f_{peak} D/U_{inf} = 4.5.

The location of the shear-layer-related peak moves toward lower frequencies with increasing elevation angle, indicating that the shear layer grows downstream from the separation location. Intensities of the spectra also increase with the Mach number. The jitter/deflection-angle spectra for a shear layer have been previously shown to follow a "ρM^2"-law [2,4]. These spectra further validate this scaling law.

The spectra are re-plotted as a function of the elevation angle for a fixed Mach number in Figure 3. For a fixed Mach number, spectra are approximately the same at a range of low frequencies between 80 and 300 Hz, indicating strong tunnel-related mechanical vibrations, which should be independent of the elevation angle. Spectra monotonically increase with increasing elevation angle, indicating that the optical aberrations caused by the shear layer become stronger with increasing looking-back angle, consistent with the expected optical character of a shear layer. The location of the shear layer peak moves toward lower frequencies with increasing elevation angle, from 1 kHz to 0.5 kHz for M = 0.3, from 1.3 to 0.8 for M=0.4 and 0.4 and from 1.8 kHz to 0.9 kHz for M = 0.5. Again, this is consistent with the shear layer structures growing in size as they convect downstream. All trends are quite similar to results for optical jitter/deflection-angle spectra around hemispheres [7]. The increasing optical signal with the elevation angle going up is not only due to the shear layer structures growing with downstream location (i.e., greater look-back angle) but also because of the fact that the laser beam is traversing the shear layer at ever-higher oblique angles, increasing its optical propagation path length due to oblique propagation (c.f. below).
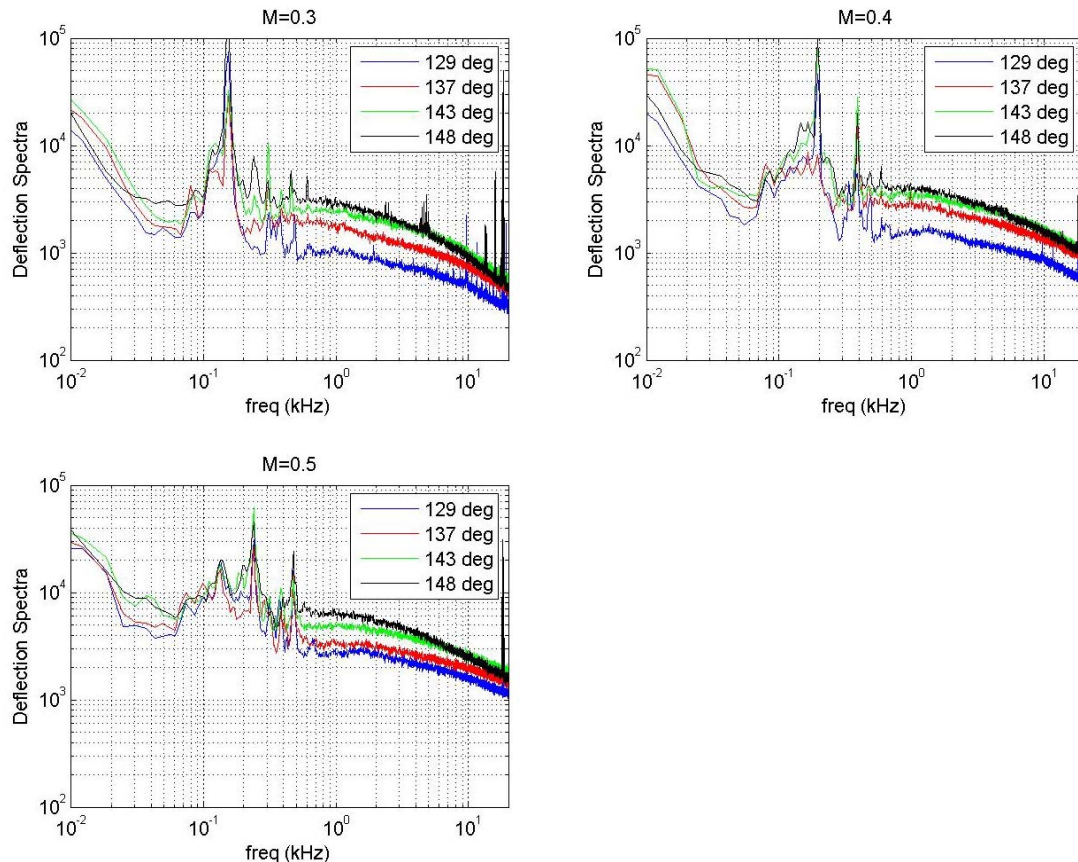

Figure 3. Optical deflection/jitter-angle spectra for different incoming Mach numbers as a function of the elevation angle. The horizontal axis is frequency in kHz.

B.   Relation between deflection-angle spectra and OPD$_{rms}$.

Mechanically-induced vibrations from the tunnel motor impose significant amounts of contamination at the low-frequency end of the deflection-angle spectra and partially corrupt the aero-optical signal. In order to remove this mechanical-vibration corruption, one needs to know the correct, uncorrupted behavior of the deflection-angle spectrum at the low-frequency end to properly filter it out.

To derive a proper high-pass filter, it is helpful to revisit how Malley probe data are used to construct a meaningful optical figure-of-merit. Malley probes measure 1-D jitter/deflection-angle spectra, $P_\theta(f) = \langle \hat{\theta}(f)\hat{\theta}^*(f)\rangle$, but a typical figure-of-merit for aero-optics is OPD_{rms} for a given aperture size, Ap. These quantities are related as follows: Since the square of the RMS Optical Path Difference is identical to the square of the RMS wavefront distortion from its mean, i.e., $OPD_{rms}^2 \equiv W_{rms}^2$, the OPD_{rms} is related to the 1-D wavefront power spectrum, $P_W(k) = \langle \hat{W}(k)\hat{W}^*(k)\rangle$, as

$$OPD_{rms}^2 \equiv \frac{1}{2\pi}\int_{-\infty}^{\infty} P_W(k)dk ,\tag{1}$$

where $\hat{W}(k)$ is the Fourier transform of a 1-D wavefront distortion, $W(x)$. But the jitter/deflection angle, θ, is the spatial derivative in the streamwise direction of the wavefront,

$$\theta(x = U_c t) = \frac{dW(x = -U_c t)}{dx} = -\frac{1}{U_c}\frac{dW(t)}{dt} .$$

Here the frozen-flow convective hypothesis is applied with U_c being the convective speed. The deflection power spectrum can be computed from the wavefront power spectrum as $P_\theta(f) = \left(\frac{2\pi f}{U_c}\right)^2 P_W(f)$. Substituting this expression into Eq. (1) we get,

$$OPD_{rms}^2 = \frac{1}{2\pi}\int_{-\infty}^{\infty} P_W(k)dk = \int_{-\infty}^{\infty} P_W(f)df = \int_{-\infty}^{\infty}\left(\frac{U_c}{2\pi f}\right)^2 P_\theta(f)df = U_c^2 \int_{-\infty}^{\infty}\frac{P_\theta(f)}{(2\pi f)^2}df$$
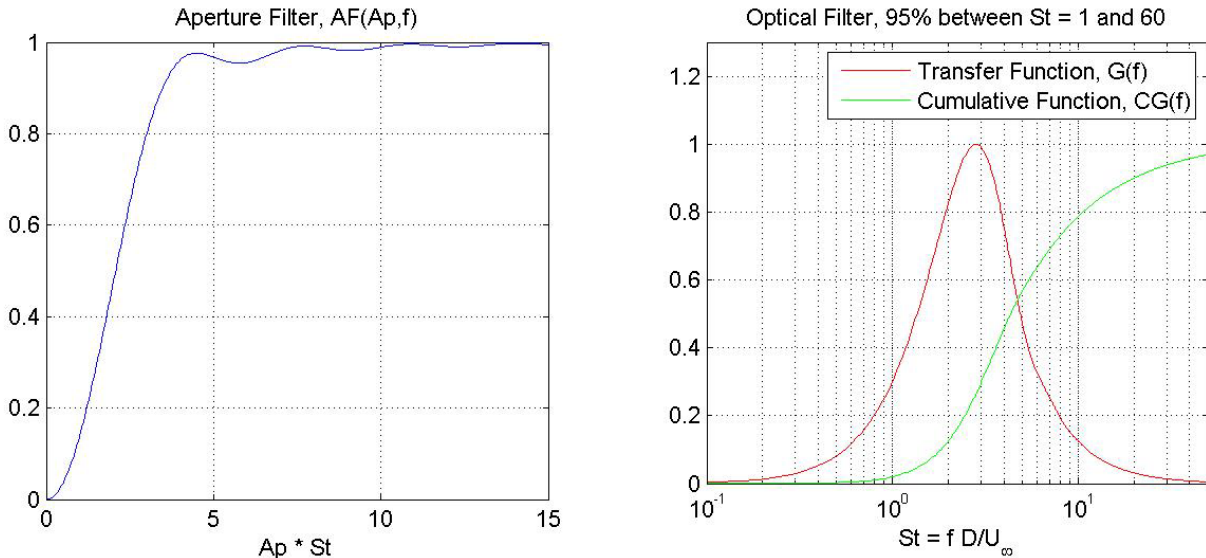

Figure 4. Left: Aperture filter. Right: Optical transfer and cumulative functions.

The derived expression is valid only for an infinite aperture. In [8] it was shown that for finite apertures, the above expression should be modified by including a 1-D aperture filter, $AF(Ap, f)$, see Figure 4, left,

$$OPD_{rms}^2(Ap) = U_c^2 \int_{-\infty}^{\infty} AF(Ap, f)\frac{P_\theta(f)}{(2\pi f)^2}df = \int_0^{\infty} G(Ap, f)P_\theta(f)df ,\tag{2}$$

where $G(Ap, f) = \frac{2U_c^2}{(2\pi f)^2}AF(Ap, f)$ is a transfer function between the deflection angle spectrum and the apertured $OPD_{rms}(Ap)$. Figure 4, right, shows the transfer function, $G(f)$, normalized by the maximum value for $Ap = 1/3\ D$ as

a function of $St = fD/U_\infty$, where D is a turret diameter and U_∞ is the freestream speed ($U_c = 0.8 U_\infty$). The

normalized cumulative transfer function, $CG(f) = \int_o^f G(x)dx / \int_o^\infty G(x)dx$, is also plotted in Figure 4, right. The

transfer function is essentially a band-pass filter, centered around St = 3. The low-frequency cut-off is due to aperture effects, where very low frequencies are present essentially as tip-tilt and therefore are removed from the final result under the presumption that a Fast Steering Mirror would be present in the beam-control system for a laser. The high-frequency cut-off is due to the integral relation between the jitter/deflection-angle signal and the wavefront. Therefore, Eq. (2) shows that the measured optical quantity, the jitter/deflection-angle spectrum, should be, in effect, *band-pass filtered* in order to calculate the level of aero-optical aberrations, OPD$_{rms}$, for a given aperture size.

From the cumulative function, $CG(t)$, see Figure 4, right, it is clear that for this aperture, 95% of the "filtered energy" is located between St = 1 and 60. Therefore, the exact shape of the low-pass filter (or more accurately, the fit) which is applied to the measured deflection angles to compensate for vibration contamination is in fact *irrelevant* below $St = 1$ (and above $St = 60$) as long as all non-physical components, like vibrations, are removed or highly suppressed by the empirical low-pass filter. Direct numerical calculations confirm these results. Two different filters were applied to remove vibration-related low frequencies, see Figure 5. The resulting OPD$_{rms}$ after applying these two filters differ by less than 6%. So, all data reported below were processed by applying Filter # 1.
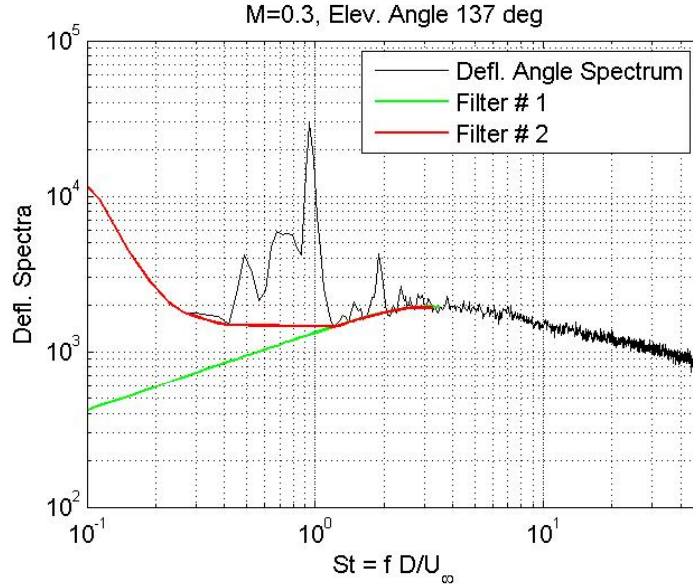

Figure 5. Deflection angle spectrum and two different low-pass filters.

High-pass filter # 1, $F(f)$, was constructed as follows,

$$F(f) = \begin{cases} \dfrac{P_\theta(f_{cut})\left(\dfrac{f}{f_{cut}}\right)^n}{P_\theta(f)}, & f < f_{cut} \\ 1, & f \geq f_{cut} \end{cases}.$$

The cut-off frequency was chosen to be $f_{cut}D/U_\infty = 4.0$. The filter was then applied to the time-dependent data as discussed earlier. Several values of n between 1 and 2 were tested and it was found that the resulting apertured OPD$_{rms}$ did not change much, so the conservative value of $n = 1$ was chosen for the high-pass filter $G(f)$.

After applying the high-pass filter, average levels of optical distortions, OPD$_{rms}$, were computed for the aperture size of Ap = 0.2 m; the OPD$_{rms}$ results are given in Table 1 and plotted in Figure 6, left, versus $\rho/\rho_{SL} M^2$ (ρ_{SL} – sea-level density) for different elevation angles. As can be seen in Figure 6, left, for all elevation angles OPD$_{rms}$ approximately follows the "ρM^2"-dependence.

Table 1. Baseline OPD$_{rms}$ (microns)

	129 deg	137 deg	143 deg	149 deg
M=0.3	0.064	0.070	0.094	0.098
M=0.4	0.085	0.119	0.143	0.143
M=0.5	0.147	0.173	0.218	0.251

For "similar" subsonic flows, levels of optical aberrations are proportional to the freestream density, the square of the incoming Mach number and the turret size, D, OPD$_{rms} \sim \rho M^2 D$. To check this self-similarity, the optical results were re-plotted in Figure 6, right, in a self-similar form, OPD$_{rms}$ /($\rho M^2 D$), versus the elevation angle, γ, for all Mach numbers. Also, the "oblique angle" effect, OPD$_{rms} \sim 1/\sin(\gamma)$ is shown in Figure 6, right, as a dashed line. For all Mach numbers and elevation angles the data approximately collapse around "$1/\sin(\gamma)$"-curve, giving additional validity to the comment made earlier that part of the increase is due to a longer optical path through the shear layer for oblique propagation.
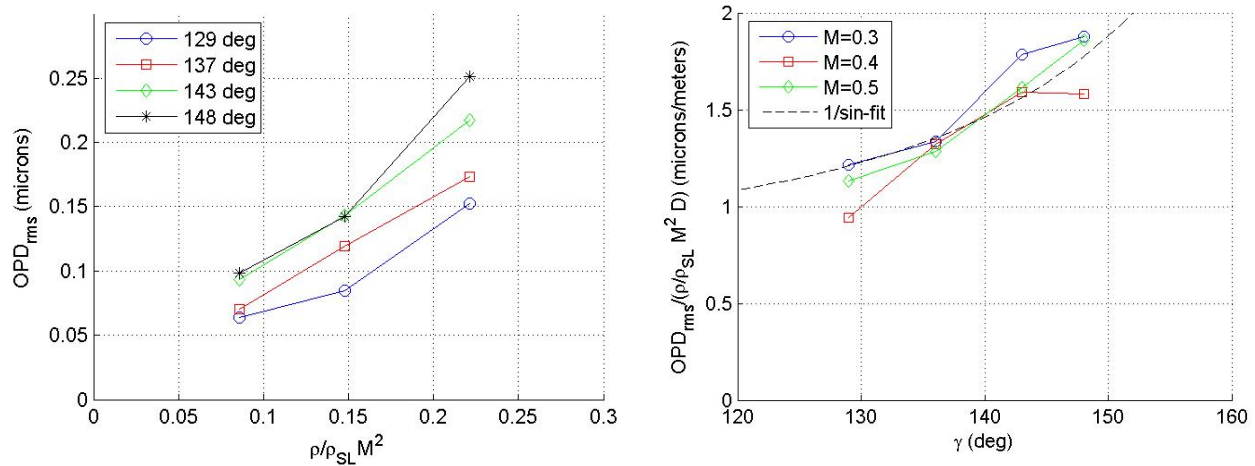

Figure 6. Left plot: Baseline OPDrms versus $\rho/\rho_{SL}M^2$ for different elevation angles. Right plot: Baseline optical data re-plotted in a self-similar form, OPD$_{rms}$ /($\rho M^2 D$) versus elevation angles for all Mach numbers.

Summarizing, for $0.3 < M < 0.5$ and elevation angles between 130 and 150 degrees, levels of optical distortions imposed on the laser beam can be approximately described as

$$OPD_{rms} = 0.95 \text{ x}10^{-6} \, (\rho/\rho_{SL}) \, M^2 D \, / \sin(\gamma).$$

This empirically-obtained result can be used to estimate optical aberrations over hemisphere-on-cylinder turrets for look-back elevation angles in the zenith plane for different altitudes (freestream density), Mach numbers and turret sizes.

C. Effect of Active Flow Control on the Aero-Optical Environment.

1. OPD$_{rms}$ results.

The same four elevation angles and Mach numbers that were investigated for the baseline case were investigated for eight selected actuation cases. The actuators' principle of operation, location and arrangements are described in [1]; they were zero-mass, blowing-suction type piezo actuators often referred as synthetic jet actuators [9]. The actuators were placed flush with the turret surface upstream of the conformal window edge; a total of 36 individually-addressable actuators were distributed in three rows around the window circumference, such that the first row (closest to the window) consisted of 15, the second of 14, and the third of 7 actuators, see Figure 7. As described in [1], these actuator devices manipulate the boundary layer on top of the hemisphere and delay/modify the separation location, thus moving the shear layer formation farther downstream and potentially improving the optical environment at look-back elevation angles. The actuators' orifices were oriented along the local free stream, injecting streamwise vorticity into the boundary layer.

Regardless of strength, in all cases the actuators operated with a suction-blowing frequency of 1.6 kHz. A total of 8 actuation cases were tested; see Table 2 for a complete description of actuation cases. The Malley probe jitter data were high-pass filtered in the same manner as was used for the baseline data and each case compared to the baseline aero-optical OPD_{rms} results.
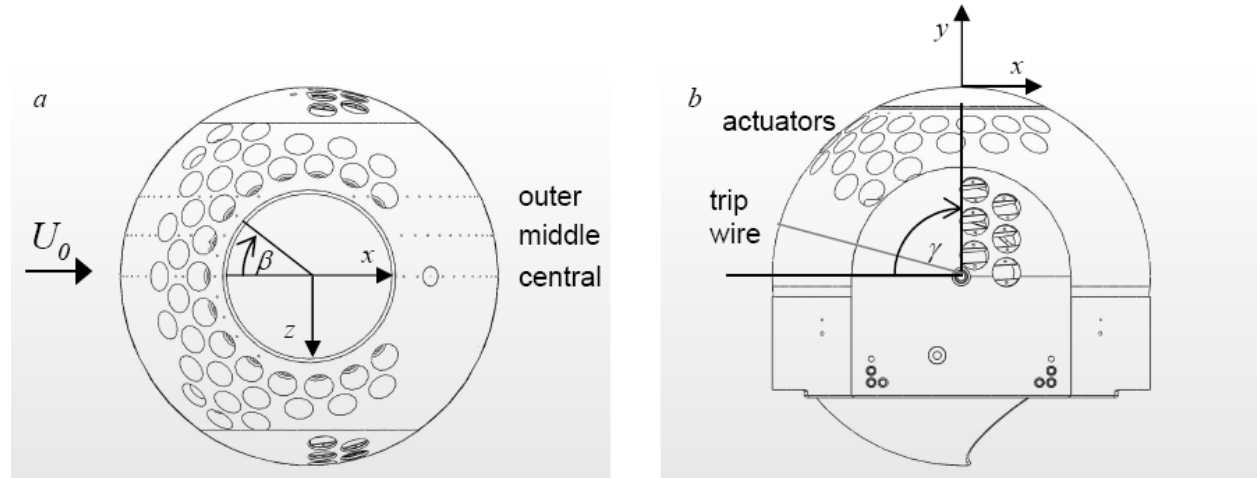

Figure 7. Top (*a*) and side (*b*) views of the turret model with actuators.

Table 2. Actuation cases tested.

Case #	Description
1	all actuators ON @ jet mean velocity ~ 51 m/s
2	all actuators ON @ jet mean velocity ~ 45 m/s
3	all actuators ON @ jet mean velocity ~ 32 m/s
4	2 farthest downstream actuators turned OFF @ jet mean velocity ~ 51 m/s
5	4 farthest downstream actuators turned OFF @ jet mean velocity ~ 51 m/s
6	6 farthest downstream actuators turned OFF @ jet mean velocity ~ 51 m/s
7	8 farthest downstream actuators turned OFF @ jet mean velocity ~ 51 m/s
8	10 farthest downstream actuators turned OFF @ jet mean velocity ~ 51 m/s

The overall OPDrms results for all eight cases at each of the elevation angles are given in Table 3 as a ratio, $(OPD_{rms})_{actuated} / (OPD_{rms})_{baseline}$. Where no number is given in the Table 3, this represents a case where no data were taken. As can be seen in Table 3, every case tested for M = 0.3 showed improvement in OPD_{rms} (i.e., all are less than 1.0); however, this cannot be said for the M = 0.4 cases. As can be seen in Table 3, the M = 0.5 is a much reduced set of tested cases, many eliminated by their effectiveness at M = 0.4. In the fewer set at M = 0.5, all showed some improvement, albeit less than at M =0.4 with one exception, Case # 1 at 129 degrees.

It should be noted that in many cases the improvement over the baseline was quite large. At M = 0.3, the reduction in OPD_{rms} at 137 degrees, for example, Case # 1 yielded a 34% improvement and at M = 0.4 the improvement dropped by only 4% to a 30% improvement. This reduction in OPD_{rms} is even more significant to the far-field intensity, since the far-field intensity improvement goes approximately as

$$\frac{I}{I_0} = \exp\left\{-\left(\frac{2\pi OPD_{rms}}{\lambda}\right)^2\right\} \tag{3}$$

where I is the on-axis intensity after tilt removal, divided by the diffraction limited intensity, I_0, and λ is the laser wavelength. Finally, Figure 9 gives the comparison of Case # 1 to the baseline for each angle and all three Mach numbers in non-dimensional form.

Table 3. Relative reduction in OPD$_{rms}$ for all actuation cases.

		129 deg	137 deg	143 deg	149 deg
M=0.3	Case #1	0.92	0.66	0.76	0.72
	Case #2	0.90	0.70	0.70	0.68
	Case #3	0.85	0.79	0.70	0.75
	Case #4	0.87	0.67	0.75	0.70
	Case #5	0.80	0.69	0.64	0.76
	Case #6	0.78	0.69	0.71	0.66
	Case #7	0.79	0.68	--	0.69
	Case #8	--	0.69	--	0.63
M=0.4	Case #1	0.95	0.70	0.79	0.85
	Case #2	1.00	0.73	0.81	0.86
	Case #3	1.07	0.84	0.90	0.97
	Case #4	0.96	0.73	0.82	0.88
	Case #5	0.88	0.71	0.86	0.87
	Case #6	1.09	0.69	0.83	0.86
	Case #7	1.00	0.70	0.79	0.87
	Case #8	1.00	--	0.76	0.88
M=0.5	Case #1	0.80	0.85	0.94	0.88
	Case #2	--	0.91	--	--
	Case #3	--	0.92	--	--
	Case #4	--	0.86	--	--
	Case #5	--	0.88	--	--
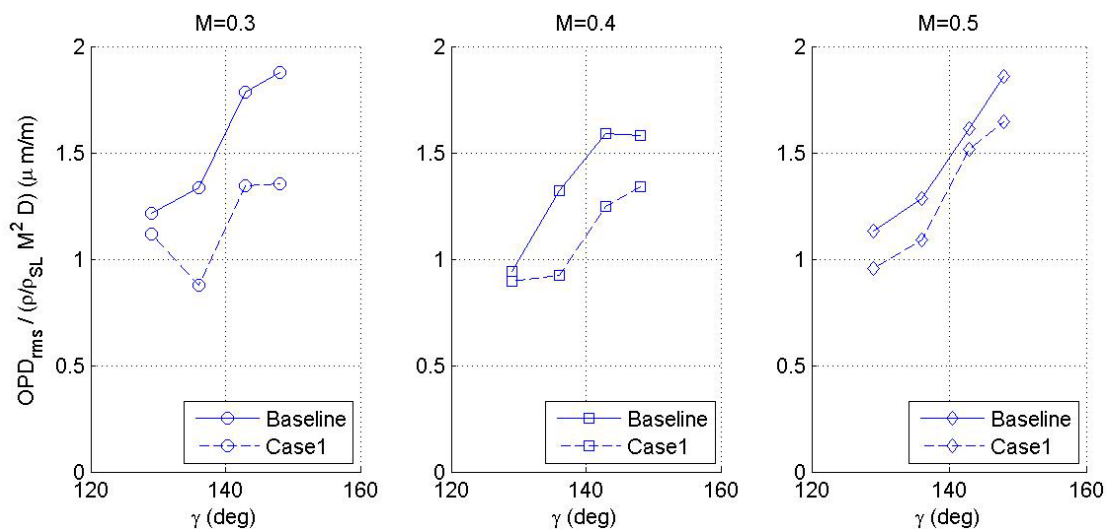
Figure 9. Normalized Baseline and Actuation Case # 1 optical data, OPD$_{rms}$ /(ρM^{2}D), versus elevation angles for all Mach numbers.

2. Spectra Results.

A detailed comparison of the jitter spectra with the baseline spectra for each case was also performed. For brevity, only Case # 1 will be discussed here as a representative example of all the spectra for the cases that showed improved aero-optical environments. Figure 10, 11 and 12 present detailed jitter spectra comparisons between case # 1 and the baseline for Mach numbers of 0.3, 0.4 and 0.5, respectively. Except for the 143 degree case at M=0.4, every actuated spectra shows a spike in the actuator-spectra at 1.6 kHz to a greater or lesser extent. This spike indicates that the actuators are introducing well-defined structures into the boundary layer that are responsible for keeping the flow attached (i.e. preventing the separation present in the baseline flow); however, these structures are aberrating as will be discussed in more details below.
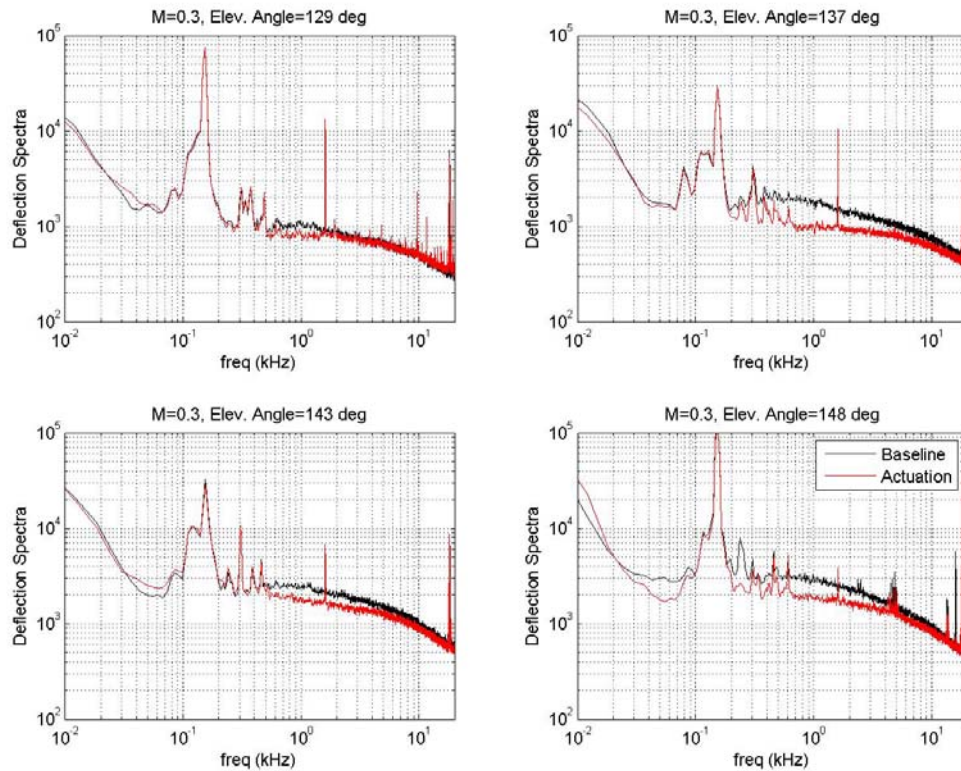
Figure 10. Deflection/jitter spectra for baseline and actuated cases at different elevation angles. Incoming M = 0.3.

Albeit actuation introduces aberrating structures into the flow at the actuator frequency, the overall effect of the actuation is a broad reduction in the jitter (and concomitant contribution to OPD_{rms}) over the broad frequency range. In particular, as was discussed with regard to Figure 4, the reduction in deflection angle spectra at frequencies between 0.2 and 10 kHz has the largest effect on the OPD_{rms}. These spectra also demonstrate that the actuation mostly affects frequencies below the actuation frequency of 1.6 kHz and at higher frequencies the actuation spectra are affected less by the actuation and approach the spectra of the baseline.

At the lowest elevation angle of 129 degrees the actuation was found to be only marginally effective, providing improvement in optical signal between 5% and 20%. A possible reason for this is that the actuators for this elevation angle were located too far upstream from the separation line and therefore had a lesser effect on modifying the separation region. Also, it is worth noting that the absolute levels of OPD_{rms} are relatively low to begin with.

Finally, it is of interest to quantify the amount of aberration that the introduction of the 1.6 kHz structures has on the optical environment. To address this question, a narrow band-pass filter was placed around the each jitter spectra centered on 1.6 kHz for the Case # 1 data and the OPD_{rms} computed for only the notched spectra. The contribution of these aberrating structures to overall OPD_{rms} were found to range from 1% to 7% of the no-notch OPD_{rms}. That is to say, if in the case of 137 degrees at M = 0.3, for example, the 34 % reduction in OPD_{rms} could have been a 41% reduction had the optical effect from 1.6 kHz aberrating structures been somehow removed.
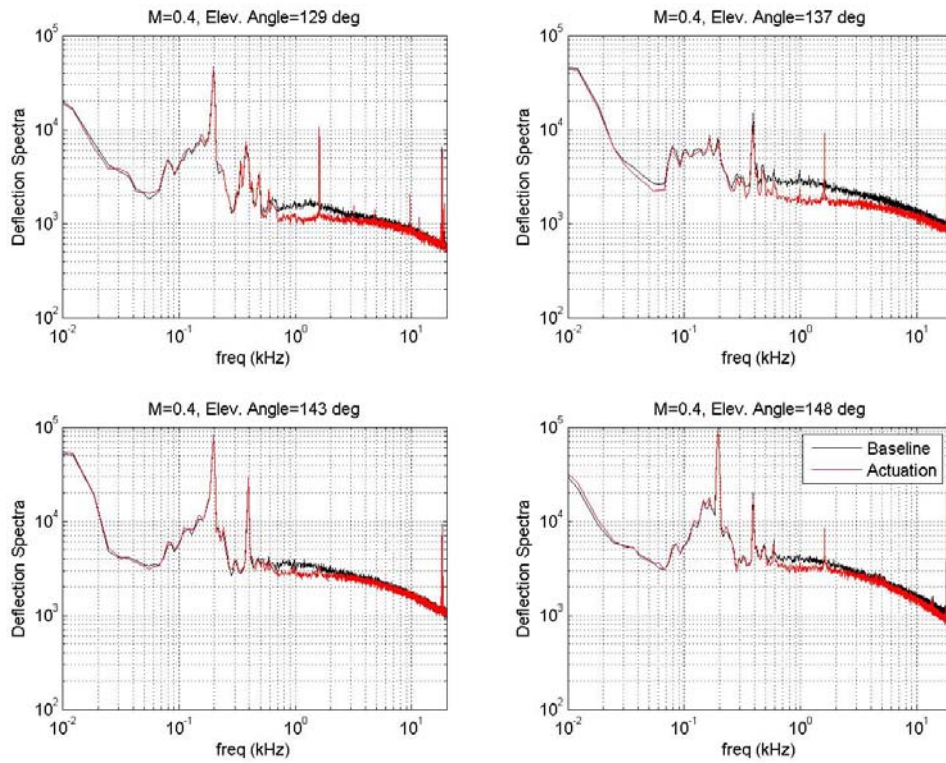
Figure 11. Deflection/jitter spectra for baseline and actuated cases at different elevation angles. Incoming M = 0.4.
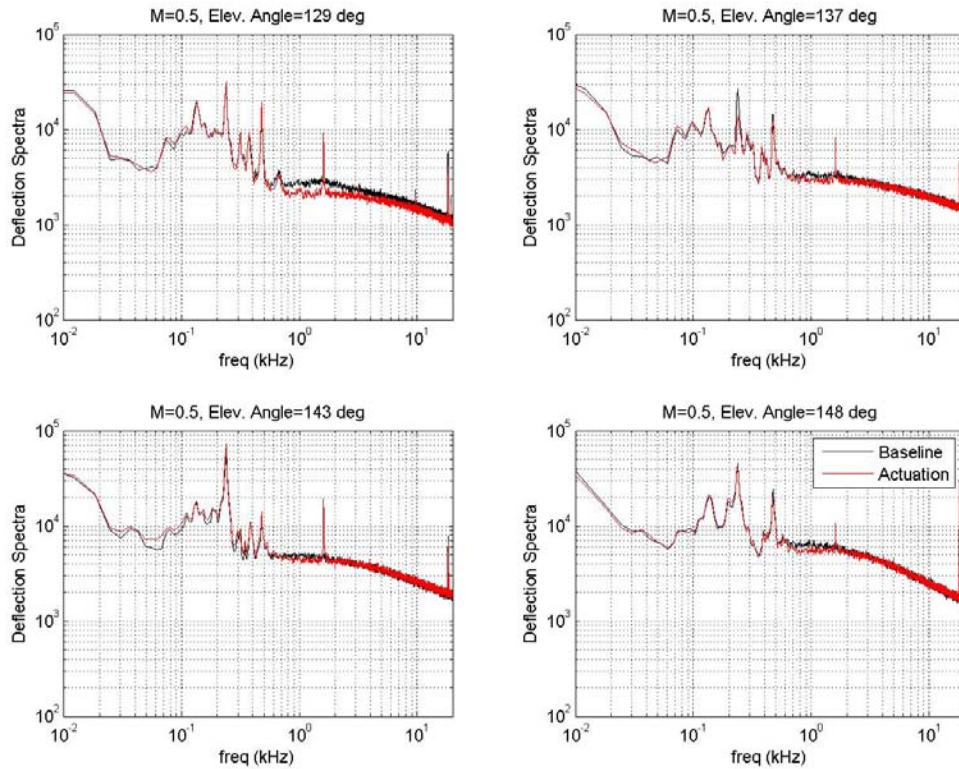

Figure 12. Deflection/jitter spectra for baseline and actuated cases at different elevation angles. Incoming M = 0.5.

IV.   Conclusions

This paper, a companion to Part I [1], has presented the aero-optical environment impact of eight cases of synthetic-jet, active-flow-control devices implemented onto a generic turret in Mach 0.3 to 0.5 flow. The general conclusion that can be drawn is such actuation can have favorable impacts on aero-optical environment of a laser propagated from the turret. As was clearly apparent, different configurations are more effective at different elevation angles. One could envision a scheduled actuation keyed to specific angles that could take advantage of the best case at each angle and/or Mach number.

This paper has also specifically addressed the often cited concern of any flow control approach; what is the possible optical degradation associated with the flow-control approach's introduction of fluid structures into the flow? At least in the present case, we can state that the introduced structures are aberrating but that the degradation introduced can be overcome by the overall improvement in the OPD_{rms}. The statement must be tempered by the cases where actuation actually made the optical environment worse. Finally, because the structures introduced into the flow by the actuation used here are so narrowly centered on the actuation frequency, there is a chance that they could be removed using a feed-forward, adaptive-optics approach similar to that demonstrated with a regularized shear layer in [10]. This suggestion, too, must be tempered by the fact that at best Malley-probe data present only a one-dimensional cut of a wavefront and, as has been shown in [2], lose applicability the farther one gets from the measurement location; in the present case the results have been extended to the extremities of the aperture based on the measurements made at the center of the aperture.

Acknowledgment

References

[1] B. Vukasinovic, A. Glezer, S. Gordeyev, E. Jumper and V. Kibens, "Fluidic Control of a Turret Wake, Part I: Aerodynamic Effects", 47th AIAA Aerospace Sciences Meeting, 5-8 Jan, 2009, AIAA Paper 2009-0816.

[2] S. Gordeyev, T. Hayden and E. Jumper, "Aero-Optical and Flow Measurements Over a Flat-Windowed Turret", *AIAA Journal*, vol. **45**, No. 2, pp. 347-357, 2007.

[3] G. Sutton,"Aero-Optical Foundations and Applications", *AIAA Journal*, Vol, **23**, No. 10, pp 1525-1537, 1985.

[4] S. Gordeyev, M. Post, T. MacLaughlin, J. Ceniceros and E. Jumper, "Aero-Optical Environment Around a Conformal-Window Turret", *AIAA Journal*, vol. **45**, No. 7, pp. 1514-1524, 2007.

[5] Gilbert, J. and Otten, L.J. (eds), *Aero-Optical Phenomena*, Progress in Astronautics and Aeronautics, Vol, **80**, AIAA, New York, 1982.

[6 J. Cress, S. Gordeyev, E. Jumper, T. Ng and A. Cain, "Similarities and Differences in Aero- Optical Structure over Cylindrical and Hemispherical Turrets with a Flat Window", 45th Aerospace Science Meeting and Exhibit, Reno, Nevada, 8-11 Jan, 2007, AIAA Paper 2007-0326.

[7] B. Vukasinovic, A. Glezer, S. Gordeyev, E. Jumper and V. Kibens, "Active Control and Optical Diagnostics of the Flow over a Hemispherical Turret", 46th Aerospace Science Meeting and Exhibit, Reno, Nevada, 7-10 Jan, 2008, AIAA Paper 2008-0598.

[8]. J. Siegenthaler, S. Gordeyev and E. Jumper, "Shear Layers and Aperture Effects for Aero-Optics", 36th AIAA Plasmadynamics and Laser Conference, Toronto, Canada, 6-9 June, 2005, AIAA Paper 2005-4772.

[9] Smith, B.L. and Glezer, A.,"The Formation and Evolution of Synthetic Jets", *Phys. Fluids*, Vol. **10**, 1998, pp. 2281 – 2297.

[10] A. Nightingale, B. Mitchell, B. Goodwine and E. Jumper, "Feedforward Adaptive-Optic Mitigation of Aero-Optic Disturbances", 39th AIAA Plasmadynamics and Lasers Conference, Seattle, WA, 23-26 June, 2008, AIAA-2008-4211.